This document was prepared in conjunction with work accomplished under Contract No. DE-AC09-96SR18500 with the U. S. Department of Energy.

DISCLAIMER

Proceedings of PVP2006-ICPVT-11
2006 ASME Pressure Vessels and Piping Division Conference
July 23-27, 2006, Vancouver, BC, Canada

PVP2006-ICPVT11-93522

COMPARISON OF EXPERIMENTAL TO THEORETICAL STRAINS DURING WATER HAMMER

Robert A. Leishear
Westinghouse Savannah River Corporation
Aiken, South Carolina, 29808
803-208-8394, Robert.Leishear@SRS.gov

ABSTRACT

Experimental strains during water hammer were compared to theoretical equations for strain. These equations were derived from the basic equations of motion, which lead to equations for the hoop stress and hoop strain. In this particular case, a sudden pressure increase traveling in a pipe was measured, and the hoop strains resulting from this fluid transient were also measured. Measuring the strains at numerous locations along the pipe permitted comparison of the strains as a function of position with respect to the fluid shock wave. This comparison of strains at different positions along the pipe permits analysis the vibratory nature of the strain in the pipe wall. Essentially, the equations of motion provide an approximate technique to find the maximum stress and strain due to water hammer.

NOMENCLATURE

a	wave speed, ft/second
α	vapor fraction
D	specific damping
DVSFconst	constant
Δh	enthalpy
Δs	entropy
E	elastic modulus, psi
ε', ε'_{max}	strain, inch/inch
ε	efficiency
ft	feet
g	gravitational constant, in / second^2
gpm	gallons per minute
ID	inside diameter, inch
k	bulk modulus, psi
Ls, Lv	length, ft
NPS	national pipe schedule
OD	outside diameter, inch
psi	pounds per square inch
psia	absolute pressure, psi
p	constant
P, Pg, Pi	pressure, psi
Pr1	pressure spike
R	radius, inch
St	static stress, psi
σ	dynamic stress
σra	range stress, psi
σ_u	ultimate strength, psi
σ_e	endurance limit, psi
T	time, seconds
t	thickness, inch
τ	rise time, seconds
μstrain	micro-strain, 10^{-6} inch / inch
Vcr	critical velocity, ft / second
Vol, Volg	volumes, in^3
VS, VSI, VSF	vibrations
VSfconst	constant
VFD	variable frequency drive
ρwater, ρpipe	weight density, pounds per cubic foot
SRS	Savannah River Site
ω	frequency, radians / second
ν	Poisson's ratio
ζs, ζfl, ζ	damping ratios

INTRODUCTION

This is the third in a set of three papers describing measurements of pipe strains and pressure transients, which result from water hammer. This paper focuses on the comparison of measured pipe strains to predicted theoretical pipe strains. Earlier work (Leishear [1 and 2]) showed that vibration equations provided a good approximation to find the pipe strain in an aluminum, air filled, tube subjected to a moving shock wave. This approximation was compared to the experimental research carried out by others (Beltman, et. al. [3]), and good agreement was noted between theory and experiment. The derived vibration equations were noted to be independent of the fluid, and consequently the theory was expected to provide good agreement with experimental results. Shown in this paper, the magnitude of the pipe strains provides good agreement with theory, but other factors permit only an

approximation of the actual wave form measured during tests. To compare theory to experiment, the test setup, the experimental results, and theoretical predictions are required.

SYSTEM DESCRIPTION AND TEST SETUP

The piping system of concern to this study consists of steam condensate piping at Savannah River Site (SRS), which is described in detail in the companion paper. For the purposes of this study, the only aspects of the system description required are the measured pressure surges, the test apparatus, and various material and pipe properties required in the pipe strain calculations.

The test setup is shown in Fig. 1. A processor was used to process up to a million data points on 18 channels. One channel of the processor was used to record measurements from the pressure transducer, which had a tolerance of – 0 / + 75 psi. The transducer was inserted into ¾" tee from the 2 NPS piping under consideration. The other channels were used to record data from strain gauges, which had a tolerance of +/- 0.5% in / in. The strain gauges were attached to the piping at locations shown in Fig. 1 to measure the strain, or inches of pipe deformation per inch of length. Sample rates were 1,000,000 cycles per second for strain data and 50,000 cycles per second for pressure data. The data was automatically recorded when a selected, preset trigger level was measured. The time scale was zeroed to this pressure spike.

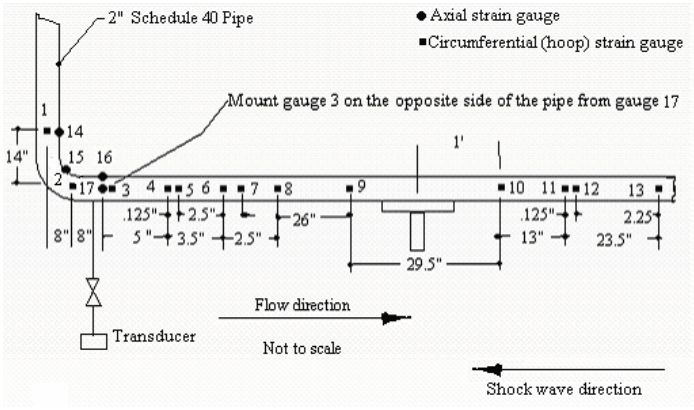

Figure 1: Test Setup

DESCRIPTION OF THE PRESSURE TRANSIENTS

Following pump startups, shock waves were initiated in the piping, which traveled upstream into the flow as shown in Fig. 1. A typical record of the pressure transients is shown in Figs. 2 - 4. Figure 2 shows the complete record of data taken when the fluid transient occurred. Figures 3 and 4 zoom in on a specific pressure spike, denoted as Pr1. Note the high frequency of the spike due to vapor collapse, which was discussed in the companion paper. The measured maximum pressure was 925 psi, but a series of pressure spikes occurred during each recorded pressure transient.

Pressures were also measured following the installation of a variable frequency drive (VFD) on the pump motor. Slow startups of the pump corrected the transient as discussed in the companion paper. A typical pressure surge is shown in Fig. 5

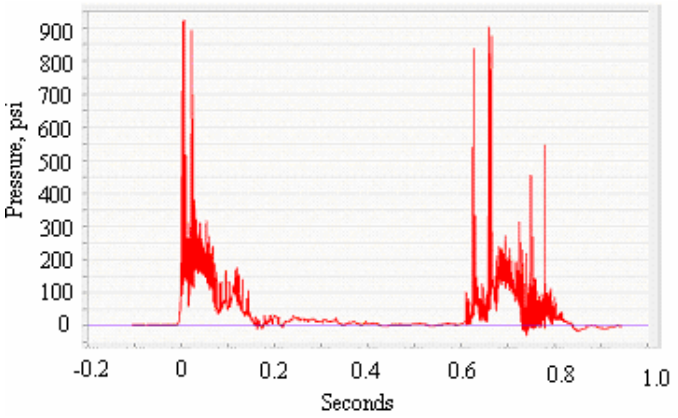

Figure 2: Typical Pressure Surge

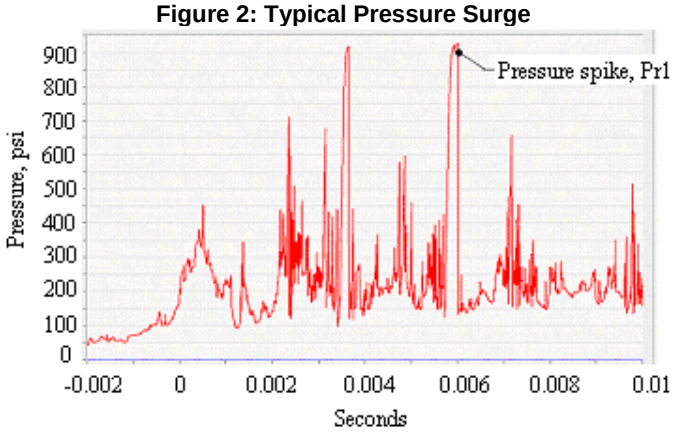

Figure 3: Typical Pressure Data (zoomed in)

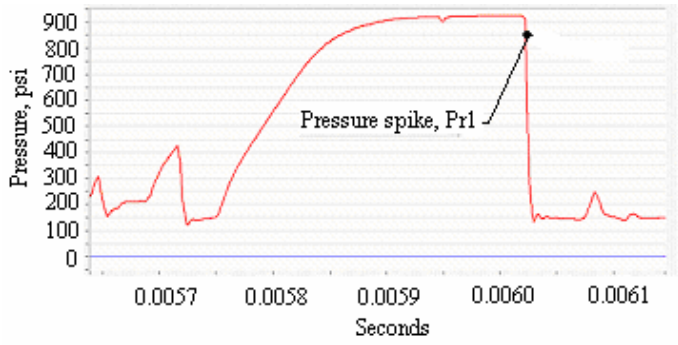

Figure 4: Pressure Data (zoomed in)

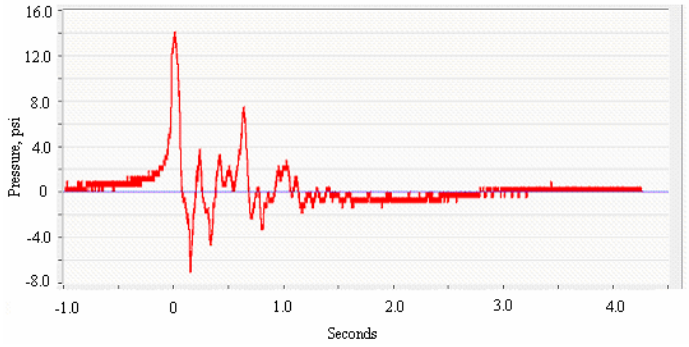

Figure 5: Typical Pressure Surge after Corrective Actions

STRAIN MEASUREMENTS

Strain measurements were taken at numerous locations before and after the installation of a VFD. After the VFD installation the strain rate measurements were low enough that they were obscured by electrical noise on the signal to the processor, as shown in Fig. 6. But before the VFD was installed, detailed test data was obtained to describe hoop strains in the circumferential direction, and some limited data was obtained to describe axial strains due to bending. Let's consider the hoop strains followed by a discussion of the axial strains.

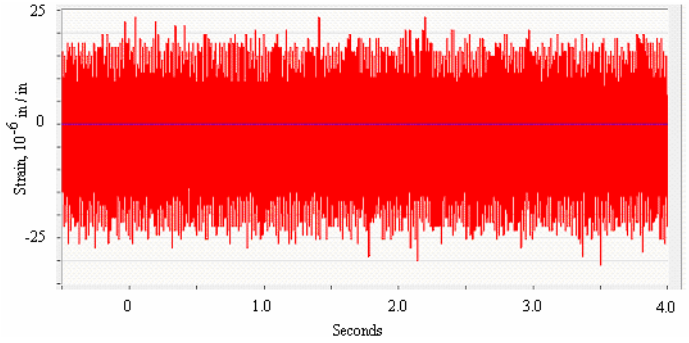

Figure 6: Hoop Strains after VFD Installation

EXPERIMENTAL HOOP STRAINS

The hoop strains were observed to travel along the pipe wall at the velocity of the fluid shock wave. Pipe strains caused by the pressure spike indicated as Pr1 in Figs. 3 and 4 are used throughout the remaining evaluation. Any one of the pressure spikes shown in the figure yields similar results, but focusing on one spike simplifies the discussion of pipe strains.

The pressure spike Pr1 travels as a shock wave at a velocity near the acoustic wave speed of water in the pipe, and will cause the pipe wall to vibrate, or breathe in and out, in the wake of the shock as it passes any point along the inner pipe wall (Leishear [1]). A strain wave moves along the pipe at the speed of the traveling shock wave.

The strain gauges located as shown in Fig. 1 were used to examine hoop strain behavior, and Figure 7 shows a typical record of measured strains. Figures 8 - 20 zoom in to display the strains associated with the pressure shock, Pr1. This series of figures shows the pipe strain at successive points along the pipe wall as the pressure wave travels upstream along the pipe. The strain rate behavior is completely described using the figures. The magnitudes of the strains vary from 580 to 800 μstrain (μstrain = 1 micro-strain), and the strain waves travel at the shock wave velocity.

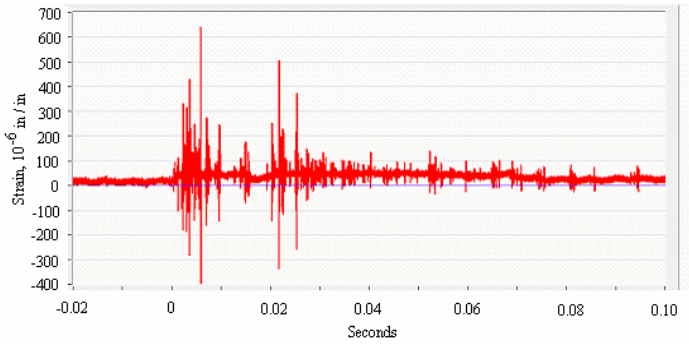

Figure 7: Typical Strain Measurements at Point 13

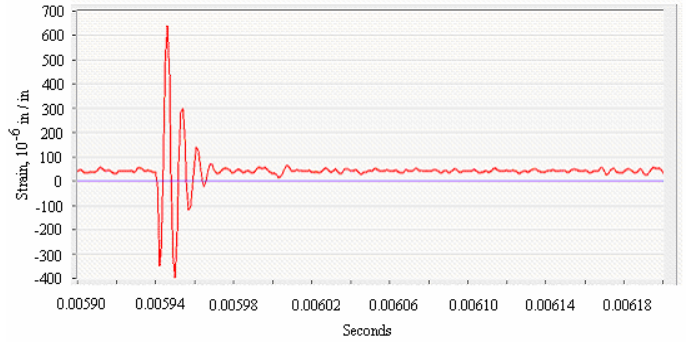

Figure 8: Typical Strain Measurements at Point 13 (zoomed in)

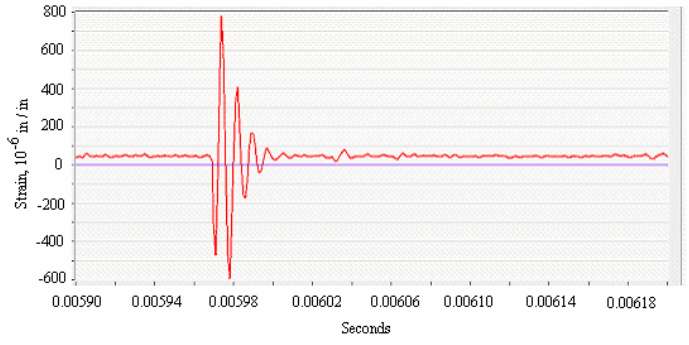

Figure 9: Typical Strain Measurements at Point 12

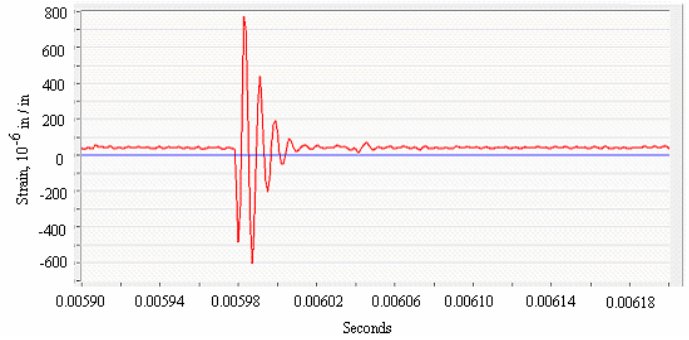

Figure 10: Typical Strain Measurements at Point 11

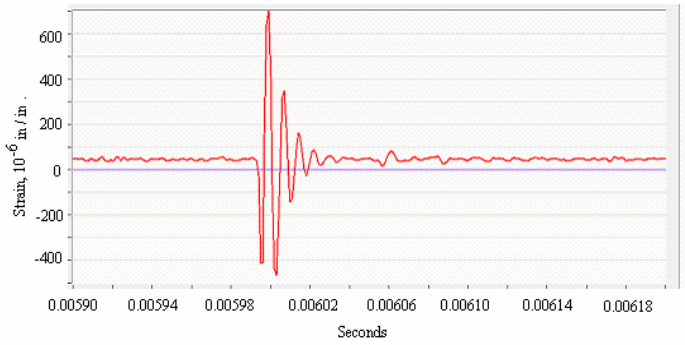

Figure 11: Typical Strain Measurements at Point 10

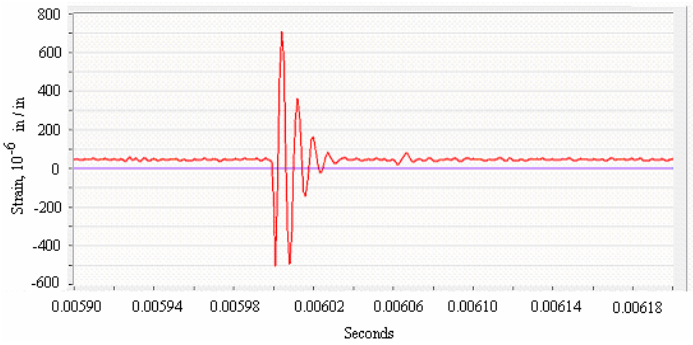

Figure 12: Typical Strain Measurements at Point 9

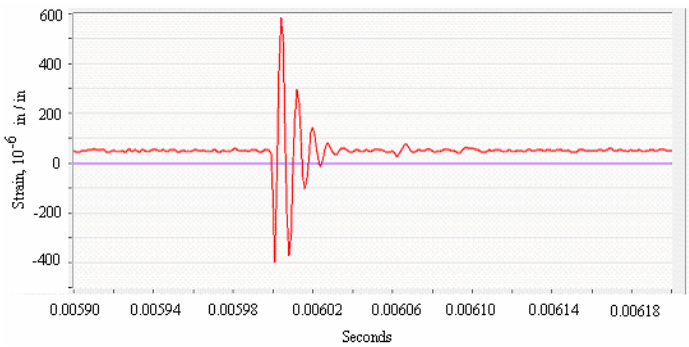

Figure 13: Typical Strain Measurements at Point 8

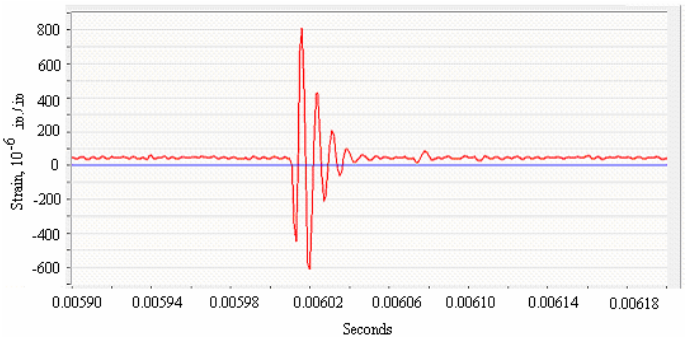

Figure 14: Typical Strain Measurements at Point 7

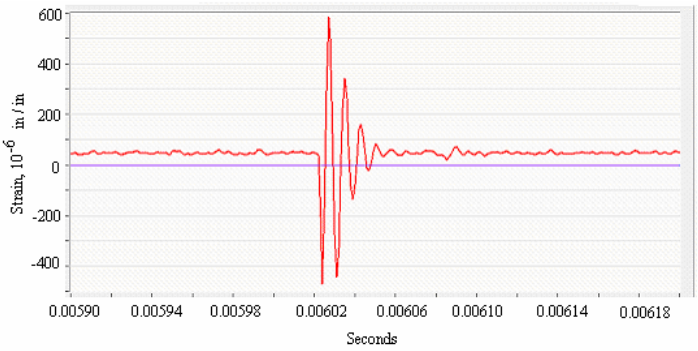

Figure 15: Typical Strain Measurements at Point 6

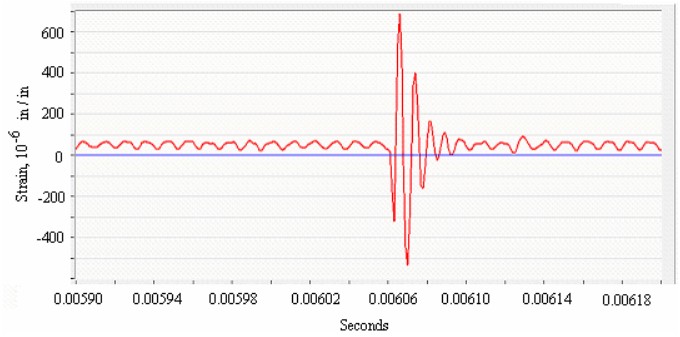

Figure 16: Typical Strain Measurements at Point 5

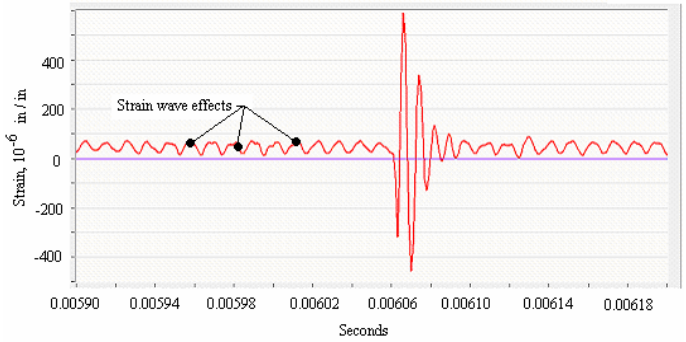

Figure 17: Typical Strain Measurements at Point 4

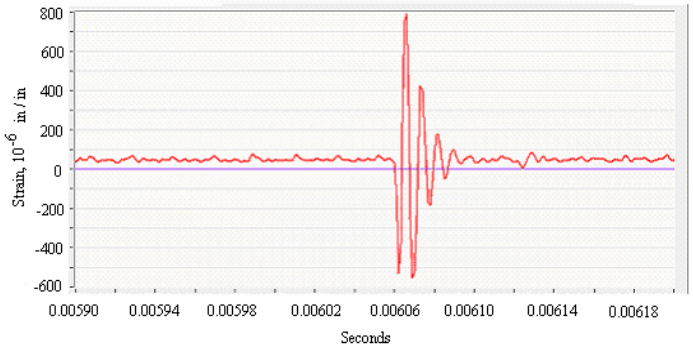

Figure 18: Typical Strain Measurements at Point 3

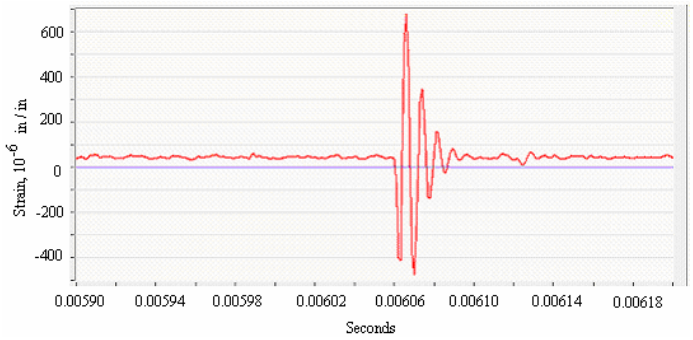

Figure 19: Typical Strain Measurements at Point 2

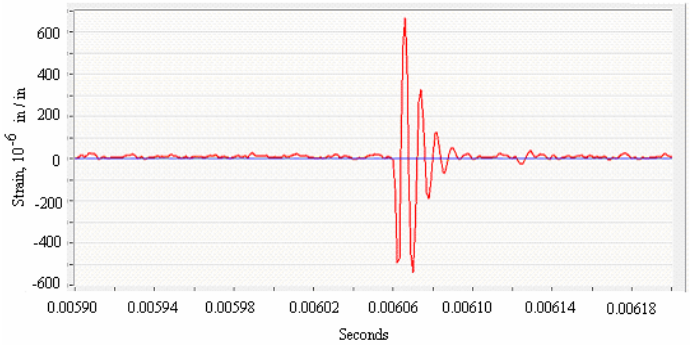

Figure 20: Typical Strain Measurements at Point 1

Shock Wave Velocity

Although the shock velocity varies along the length of the pipe, the approximate shock velocity may be found from the locations of the strain gauges and the time that strain waves act at each location. For example, the time of travel between points 3 and 13 can be found to be 0.00325 seconds from Figs. 8 and 20, and the distance between the gauges is 8.708 feet as determined from Fig. 1. The approximate shock velocity is thus

$$a = \frac{8.708}{0.00325} = 2679\_ft/sec = 32148in\_sec \qquad (1)$$

Accuracy of Results

Although the strain gauges provide accurate results, the sampling rate affects the results. For example, points 4 and 5 on the pipe were only located 1/8 of an inch from each other. The measured strains should be comparable, but they varied by 100 μstrain, or approximately 12 %. This error is due to the sample rate as shown for a typical strain measurement in Fig. 21. The maximum value depends on the time at which the sample is recorded. However, sufficient samples were obtained to ensure that the maximum measured strain was, in fact, equal to 800 μstrain.

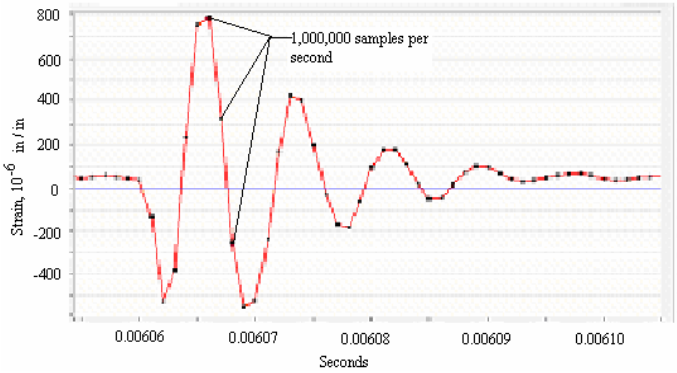

Figure 21: Effects of the Sample Rate on the Accuracy of Measured Strains

Also, the maximum strain magnitude is affected in general by the applied pressure, and this pressure was noted above to be higher than measured by as much as 75 psi, which is another potential error of 8 %. Consequently, the maximum real strain is approximately

$$\varepsilon'_{max} = 900\ \mu strain \qquad (2)$$

Strain waves also affect the maximum measured strain.

Strain Wave Effects

The effects of strain waves are observed in the figures. Strain wave effects are clearly seen in Fig. 17. In other figures, the strain waves are evident, in others the strain waves are cancelled out by other strain waves. The strain wave effects are found by comparing the maximum strain wave (100 μstrain) to the maximum strain (800 μstrain), such that the magnitude of the strain wave is 100 / 800 = +/- 0.125 times the maximum strain.

Strain waves were noted to occur throughout the pipe length at a value of $+/- \nu^2 = 2 \cdot \nu^2 = 0.168$ times the maximum strain (Leishear [1]).

$$\varepsilon'_{max} = \varepsilon' \cdot (1 + \nu^2) \qquad (3)$$

Therefore the observed strain waves are consistent with this predicted result. Strain waves also add and subtract to the maximum strain. In other words, the magnitude of the maximum strain varies not only as a function of the sample rate but varies as a function of strain wave effects. The variance in the measured maximum strain rates are attributed to these two factors. To compare the other aspects of experimental hoop strains to predicted strains, a theoretical description of the hoop strains is required.

THEORETICAL HOOP STRAINS

All of the equations needed to describe the hoop strains and hoop stresses are presented here. The derivations of these equations, detailed discussions of those derivations, and a comprehensive list of references are available (Leishear [1]). First of all, equations to relate strain to stresses, and a definition of the theoretical stress, are required to describe the hoop strains.

The hoop stress is related to the strain by Hooke's law, which for a pipe with fixed ends states that

$$E \approx \frac{\left(1-\nu^2\right)\cdot St - \nu \cdot P}{\varepsilon'} \tag{4}$$

where ν is Poisson's ratio, St is the static stress, ε' is the strain, and P is the applied pressure. Using this equation and a definition of the hoop stress defines the theoretical strain.

The hoop stress consists of a vibration preceding the shock, called a precursor vibration and an after shock vibration. The aftershock vibration is the primary vibration of concern and is the only vibration considered here. That vibration is evaluated at time equal to zero, and the equation of motion to fully describe this moving wave requires some further work. Essentially, these equations were derived from the point of view of a stationary point on the pipe wall, as opposed to a point moving with respect to the wave. The aftershock vibration at a time when the shock arrives at a point is expressed as

$$\sigma(T) = St \cdot \left(VSI(T)\big|_{0\le T<\tau} + VS(T)\big|_{T\ge\tau} + VSF(T)\big|_{T\ge\tau} \right) \tag{5}$$

where $\sigma(T)$ is the dynamic stress, and VSI(T), VS(T), and VSF(T) are vibrations due to the water hammer.

To evaluate this equation, numerous quantities were required, such as property constants for the pipe and water, and variables such as the frequency, wave speed, and damping. Once the constants and variables were found, the pipe strains were calculated using stress equations.

Material and Pipe Constants

Data from Mark [4], Keenan and Keyes [5], and ASME B31.3 [6] along with other required data is tabulated in Table 1.

Operating Temperature	178°F	Poisson's ratio, ν	0.29
Pipe wall material	P53 steel	Median radius, R	1.188
Elastic Modulus, E	28600000	Rise time, τ	2.741
Bulk modulus of water, k	319000	Shock velocity, a	30400
Water density, ρwater	0.035	Initial head , P_i	9.35
Pipe density, ρpipe	0.283	Max. pressure, P	925
Pipe outside diameter, OD	2.375	Shock velocity, a	3141
Pipe inside diameter, ID	2.067	Efficiency, ε	0.999
Pipe wall thickness, t	0.154	Enthalpy, Δh	0.273
Structural damping, ζs	0.009	Entropy, Δs	0.0001
Gravitational constant, g	386.1	Specific damping, D	1.652
Frequency, ω	168000	Fluid damping, ζfl	0.0005
Ultimate strength, σ_u	60000	Constant, DVSFconst	≈ 0
Endurance limit, σ_e	30240	Constant, VSFconst	1.1012
Critical velocity, Vcr	4604	Vapor fraction, α	0.0005
Average pressure, psia, Pg	214.7		

Table 1: Material and Pipe Data

Calculated Variables

Calculated variables are also tabulated in Table 1. The equations to find them follow.

The frequency of the hoop stress is expressed as

$$\omega = \sqrt{g \cdot \frac{\left(\frac{2\cdot k}{(R)\cdot t}\right) + \left(\frac{E}{(R)^2\cdot\left(1-\nu^2\right)}\right)}{\rho pipe + \frac{(R)\cdot\rho water}{4\cdot t}}} \tag{6}$$

The critical velocity at which resonance occurs is

$$V_{cr} = \sqrt{\frac{E\cdot t}{\rho\cdot R}} \cdot \left(\frac{1}{3\cdot\left(1-\nu^2\right)}\right)^{1/4} \tag{7}$$

The shock wave speed is

$$a = \sqrt{\frac{\frac{k\cdot g}{\rho water}}{1 + \left(\frac{k}{E}\cdot\frac{2\cdot R}{t}\right)\cdot\left[\frac{t}{R}\cdot(1+\nu) + \frac{2\cdot R\cdot\left(1-\nu^2\right)}{2\cdot R + t}\right]}} \tag{8}$$

The total volume, Vol, of the pipe is

$$Vol = \frac{\pi\cdot(ID + \Delta ID)^2}{4} \tag{9}$$

Assuming that water vaporizes, or cavitates, momentarily when the pipe wall expands yields a vapor volume, Volg, such that

$$Volg = \frac{\pi\cdot(ID + \Delta ID)^2 - \pi\cdot ID^2}{4} \tag{10}$$

The percentage of vapor, or vapor fraction, with respect to the total volume is

$$\alpha = \frac{Volg}{Vol} \tag{11}$$

Steeter [7] provides a technique to adjust the wave speed due to vapor in the water, such that the wave speed can be rewritten as

$$a = \sqrt{\frac{a^2}{(1-\alpha)\cdot\left(1+\frac{\alpha\cdot\rho water\cdot a^2}{Pg^2}\right)}} \tag{12}$$

The pressure, Pg, at which cavitation in the pipe is expected to occur is the average pressure, or approximately 200 psi, as seen in Fig. 2.

$$Pg = 200 + 14.7 \tag{13}$$

The rise time is expressed as a constant,

$$p = \frac{\pi}{\tau} \tag{14}$$

Assume that all of the water is isothermally compressed from the initial conditions to the final pressure, and further assume that the vapor volume expands adiabatically to the vapor temperature. Using the initial conditions at 178° F with a head pressure of 9.35 psi and the final conditions at 925 psi, the efficiency of compression was found using the steam tables and

$$\varepsilon = \frac{\Delta h - \Delta s}{\Delta h} \tag{15}$$

Using the efficiency, the fluid damping was found

$$\zeta fl = \sqrt{\frac{2\cdot\ln(2\cdot\varepsilon-1)^2}{\pi^2+\ln(2\cdot\varepsilon-1)^2}} \tag{16}$$

The static stress is

$$St = \frac{P\cdot ID^2\cdot\left[(2OD)^2\right]}{OD^2\cdot\left(OD^2-ID^2\right)} \tag{17}$$

The range stress is

$$\sigma ra = \sigma e\cdot\left(1-\frac{\sigma max^2}{4\cdot\sigma uts^2}\right) \tag{18}$$

Specific damping is

$$D = \left(\frac{\sigma ra}{\sigma e}\right)^{2.4} + \left(\frac{\sigma ra}{\sigma e}\right)^{8} \tag{19}$$

Thus the structural damping is

$$\zeta s = \frac{D\cdot E}{2\cdot\pi\,\sigma ra^2} \tag{20}$$

The total damping equals

$$\zeta = \zeta fl + \zeta s \tag{21}$$

Thus all of the required constants and variables are established.

Stress Equations

Once the constants and variables were found, the pipe stresses were calculated using the following stress equations and variables. Again, details of these vibration equations are discussed in the earlier work (Leishear [1]).

$$VSI(T) := St\cdot\frac{1}{1}\cdot\left[\left(\frac{p\cdot e^{-\zeta\cdot\omega\cdot T}\cdot\sin\left(\omega\cdot T\cdot\sqrt{1-\zeta^2}\right)}{\omega\cdot\sqrt{1-\zeta^2}}\cdot\frac{\omega^2-p^2}{\omega^4+4\cdot\zeta^2\cdot\omega^2\cdot p^2-p^4}\right)\right.$$

$$+\left[e^{-\zeta\cdot\omega\cdot T}\cdot\cos\left(\omega\cdot T\cdot\sqrt{1-\zeta^2}\right)\cdot\left(-1+\frac{2\cdot\zeta\cdot\omega}{\omega^4+4\cdot\zeta^2\cdot\omega^2\cdot p^2-p^4}\right)\right]$$

$$\left.+\left(\frac{2\cdot\zeta\cdot\omega\cdot\cos(p\cdot T)}{\omega^4+4\cdot\zeta^2\cdot\omega^2\cdot p^2-p^4}\right)+\frac{\left(\omega^2-p^2\right)\cdot\sin(p\cdot T)}{\omega^4+4\cdot\zeta^2\cdot\omega^2\cdot p^2-p^4}+1\right]\cdot\Phi(\tau-T) \tag{22}$$

$$VSF(T) := e^{-\zeta\cdot\omega\cdot(T-\tau)}$$

$$+\left[e^{-\zeta\cdot\omega\cdot T}\cdot\cos\left(\omega\cdot T\cdot\sqrt{1-\zeta^2}\right)\cdot\left(-1+\frac{2\cdot\zeta\cdot\omega}{\omega^4+4\cdot\zeta^2\cdot\omega^2\cdot p^2-p^4}\right)\right]$$

$$+\left(\frac{2\cdot\zeta\cdot\omega\cdot\cos(p\cdot T)}{\omega^4+4\cdot\zeta^2\cdot\omega^2\cdot p^2-p^4}\right)+\frac{\left(\omega^2-p^2\right)\cdot\sin(p\cdot T)}{\omega^4+4\cdot\zeta^2\cdot\omega^2\cdot p^2-p^4}+1\Bigg]\cdot\Phi(\tau-T) \tag{23}$$

$$VSFP(T) := e^{\zeta\cdot\omega\cdot(T-\tau)}$$

$$\left[\frac{(DVSFconst + \zeta\cdot\omega\cdot VSFconst)\cdot\sin\left[\omega\cdot(T-\tau)\cdot\sqrt{1-\zeta^2}\right]}{\omega\cdot\sqrt{1-\zeta^2}}\right]\cdot\Phi(-T+\tau)$$

(24)

$$DVSFconst := \frac{St}{2}\cdot\left[\frac{-\zeta\cdot\left[e^{-\zeta\cdot\omega\cdot\tau}\cdot p\cdot(\omega^2-p^2)\cdot\sin\left(\omega\cdot\tau\cdot\sqrt{1-\zeta^2}\right)\right]}{\omega\cdot\sqrt{1-\zeta^2}\cdot(\omega^4+4\cdot\zeta^2\cdot\omega^2\cdot p^2-p^4)}\right.$$

$$+\frac{e^{-\zeta\cdot\omega\cdot\tau}\cdot p\cdot(\omega^2-p^2)\cdot\cos\left(\omega\cdot\tau\cdot\sqrt{1-\zeta^2}\right)}{\omega^4+4\cdot\zeta^2\cdot\omega^2\cdot p^2-p^4}-\left(\frac{2\cdot\zeta^2\cdot\omega^2}{\omega^4+4\cdot\zeta^2\cdot\omega^2\cdot p^2-p^4}-1\right)$$

$$\cdot e^{-\zeta\cdot\omega\cdot\tau}\cdot\cos\left(\omega\cdot\tau\cdot\sqrt{1-\zeta^2}\right)-\left(\frac{2\cdot\zeta\cdot\omega}{\omega^4+4\cdot\zeta^2\cdot\omega^2\cdot p^2-p^4}-1\right)\cdot e^{-\zeta\cdot\omega\cdot\tau}$$

$$\cdot\omega\cdot\sqrt{1-\zeta^2}\cdot\sin\left(\omega\cdot\tau\cdot\sqrt{1-\zeta^2}\right)$$

$$\left.+\frac{2\cdot\zeta\cdot\omega\cdot\sin(p\cdot\tau)}{\omega^4+4\cdot\zeta^2\cdot\omega^2\cdot p^2-p^4}-\frac{(\omega^2-p^2)\cdot p\cdot\cos(p\cdot\tau)}{\omega^4+4\cdot\zeta^2\cdot\omega^2\cdot p^2-p^4}\right]$$

(25)

$$VSFconst := \left[\frac{e^{-\zeta\cdot\omega\cdot\tau}\cdot p\cdot(\omega^2-p^2)\cdot\sin\left(\omega\cdot\tau\cdot\sqrt{1-\zeta^2}\right)}{\omega\cdot\sqrt{1-\zeta^2}\cdot(\omega^4+4\cdot\zeta^2\cdot\omega^2\cdot p^2-p^4)}\right.$$

$$+\left(\frac{2\cdot\zeta\cdot\omega}{\omega^4+4\cdot\zeta^2\cdot\omega^2\cdot p^2-p^4}-1\right)\cdot e^{-\zeta\cdot\omega\cdot\tau}\cdot\cos\left(\omega\cdot\tau\cdot\sqrt{1-\zeta^2}\right)$$

$$\left.-\frac{2\cdot\zeta\cdot\omega\cdot\cos(p\cdot\tau)}{\omega^4+4\cdot\zeta^2\cdot\omega^2\cdot p^2-p^4}-\frac{(\omega^2-p^2)\cdot\sin(p\cdot\tau)}{\omega^4+4\cdot\zeta^2\cdot\omega^2\cdot p^2-p^4}+1\right]$$

(26)

These stress equations along with the tabulated constants and variables are required to find the total dynamic stress.

COMPARISON OF THEORY TO EXPERIMENT FOR HOOP STRAINS

Theory can be compared to experiment by considering Eq. 5. Rewriting that equation,

$$\sigma(T) = VSI(T) + VS(T) + VSF(T) \quad (27)$$

Substituting of Eqs. 3 and 4 into 27 yields

$$\sigma(T) = \frac{(1+\nu^2)\cdot(1-\nu^2)\cdot(VS(T)+VSI(T)+VSF(T)) - \nu\cdot P}{E} \quad (28)$$

substitution of terms into Eq. 28 provided the results shown in Fig. 22, which can be compared to typical experimental results shown in Fig. 23. These two figures are drawn on the same time scales for comparison. Comparative results are listed in Table 2. Note that the theoretical estimate for the maximum stress is approximately 4.5 % above the measured strain, and the frequencies are significantly in error by a factor of 2.9. Both deviations from experiment are attributed to the tacit assumptions of the model. That is, the pipe is assumed to vibrate as a thin walled cylinder.

The fact that the pipe is steel walled is important. The added stiffness due to the steel construction significantly affects the solution. In previous work (Leishear [2]), the predicted frequency was shown to equal the experimental frequency determined for a aluminum tube by Beltman, et. al. For the aluminum tube, frequencies were nearly equivalent for the frequency presented here, the calculated frequency provided by Beltman, and those experimental results. The only significant differences between the 2 NPS steel pipe and the2 inch diameter aluminum tube are the stiffness effects. Also, a finite element model was documented in the previous work (Leishear [1]). This model considered an 8 NPS pipe subjected to an internal shock wave. The frequency was not affected by the stiffness. Apparently, the stiffness is affected for small bore pipes due to the ratio of pipe wall thickness to diameter. An exact relationship between these dimensions and the frequency has not been established. In spite of the frequency error, the results for hoop strains presented here provide a good approximation for the upper limit of the maximum hoop strain and maximum hoop stress.

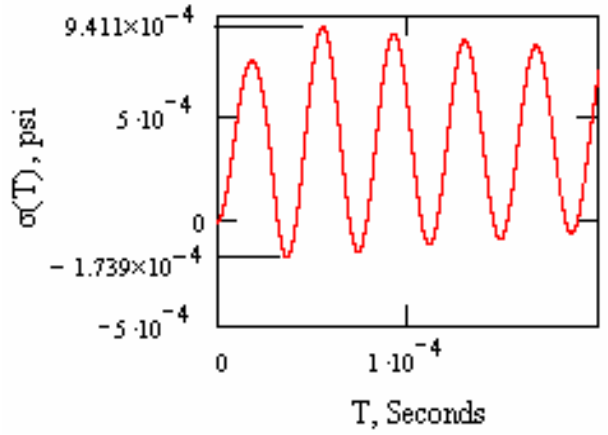

Figure 22: Theoretical Hoop Strains

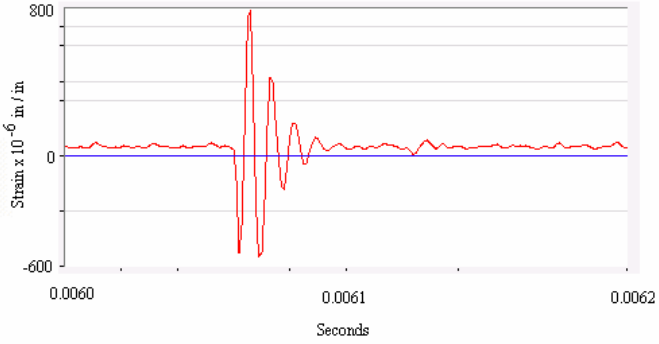

Figure 23: Typical Experimental Hoop Strains

	Theory	Experiment
Maximum μstrain	941	900
Period	$1.68 \cdot 10^{-5}$	$4.85 \cdot 10^{-5}$
Wave speed	37690	32148

Table 2: Comparison of Theoretical to Experimental Hoop Strain Data

AXIAL STRAINS

Equivalent axial and hoop strains exist simultaneously at each cross section of the pipe. That is, the pipe wall stretches in the circumferential and axial directions the same amount at the same time. To demonstrate this point, axial strains were measured at a cross section of the pipe.

The locations of the points where different strains were measured at a cross section are shown in Fig. 1 as points 3, 16, and 17. Hoop strains were measured at point 3, and the strains are shown in Fig. 18. Axial strains were measured at point 16 on top of the pipe, and the strains are shown in Fig. 24. Axial strains were also measured on the side of the pipe, and the strains are shown in Fig. 25. Comparison of these three figures shows that the strains are the same at a specific cross section of the pipe regardless of strain direction. Thus, the hoop strains and axial strains are identical at any point on the pipe wall.

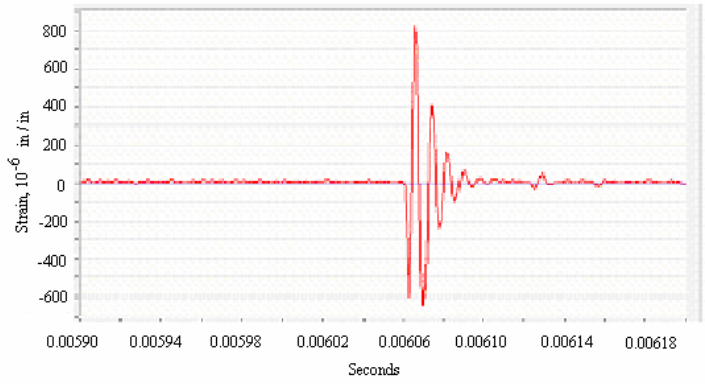

Figure 24: Axial Stresses at Point 16 on Top of the Pipe

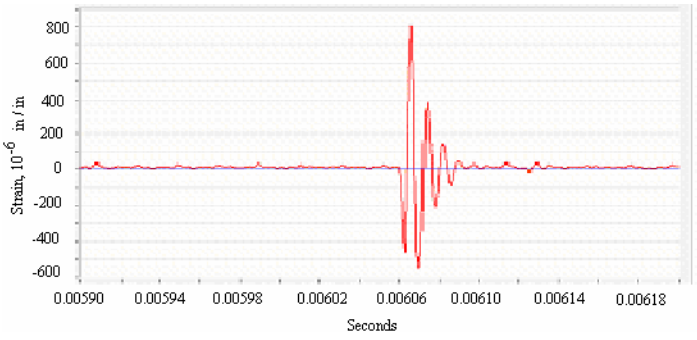

Figure 25: Axial Stresses at Point 17 on the Side of the Pipe

STRAINS DUE TO BENDING

To evaluate bending, a longer period of time needs to be examined to ensure that both lower and higher mode bending frequencies are considered. The same cross section was considered for bending that was considered for axial stresses, except that a different sample rate was used to obtain the data. Hoop stresses were measured at point 3 and axial stresses were measured at points 16 and 17. Figures 26 - 28 show strains for the entire 5 second sample. Figures 29 – 31 zoom in on the data.

Vibration modes of a structure are typically excited near the frequency of the excitation. That is, the frequency of the forcing function, or applied load, will be of a magnitude near the modal frequency of the structure. Specifically, if an excitation force is ¼ of a structure's modal frequency, that modal frequency will be excited. That is, high frequency forces cause high frequency responses. This statement is evidenced by Figs. 26 -28. The figures are nearly identical. If a low frequency modal vibration was excited, the strain gauge on top of the pipe would be flexed, and a change in vibration would be observed, which did not occur. Similarly, inspection of Figs. 29 – 31 reveals that there are no significant higher mode bending frequencies excited either. In other words, experimental data shows that higher mode bending frequencies are negligibly affected by high frequency excitation.

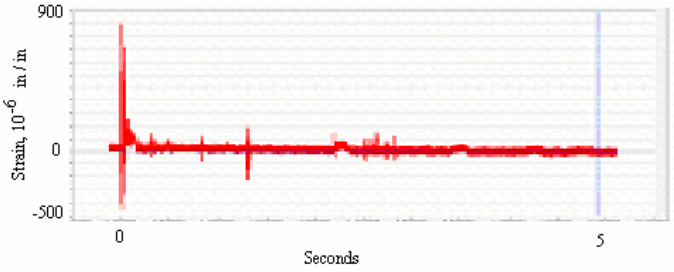

Figure 26: Hoop Strain at Point 3

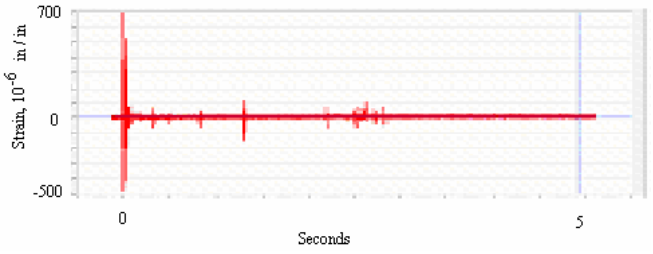

Figure 27: Axial Strain at Point 16 on Top of the Pipe

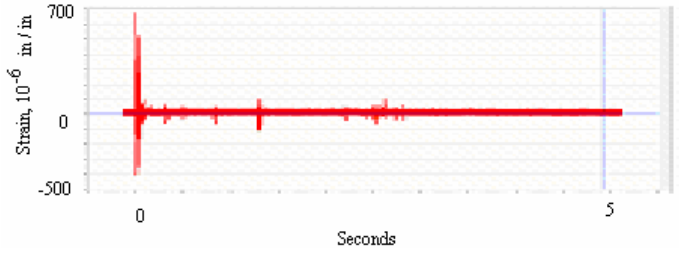

Figure 28: Axial Strain at Point 17 on the Side of the Pipe

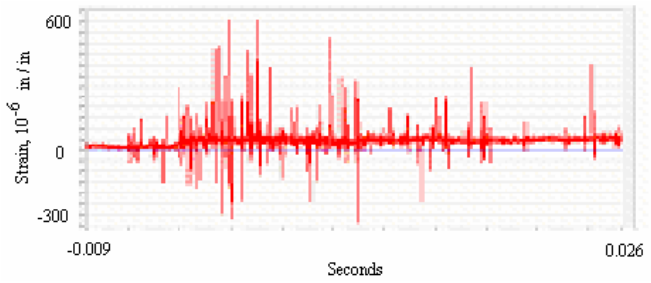

Figure 29: Hoop Strain at Point 3

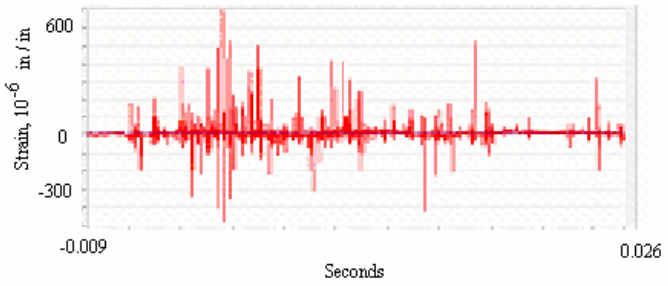

Figure 30: Axial Strain at Point 16 on Top of the Pipe

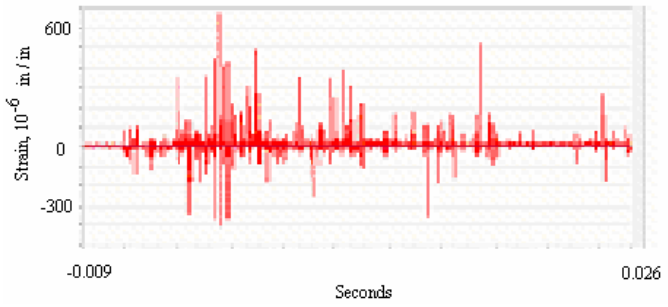

Figure 31: Axial Strain at Point 17 on the Side of the Pipe

CONCLUSION

A recently developed theory was compared to experimental data to describe stresses and strains during water hammer. Predicted maximum hoop strains were in good agreement with experiment, even though predicted vibration frequencies for the hoop strains were significantly in error due to flexural stiffness of the pipe wall. Accordingly, this model is useful in approximating maximum pipe strains and pipe stresses, which accompany water hammer incidents. Axial strain measurements indicated that bending strains caused by high frequency pressure spikes were negligible with respect to the hoop strains. Also, an axial strain parallel to the hoop strain was measured, which was equivalent in magnitude to the hoop strain. Effectively, the shock wave due to water hammer stretches the pipe wall in perpendicular directions as the wall vibrates in the wake of the shock.

ACKNOWLEDGEMENTS

Numerous SRS personnel contributed to this research. Among them are M. Wood, G. Reeves, and C. Fulghum who installed the test equipment and provided raw test data.

REFERENCES

[1] Leishear, R. A., 2005, "Dynamic Stresses During Structural Impacts and Water Hammer", PhD Dissertation, University of South Carolina, pp.1- 188.

[2] Leishear, R. A., 2005, "Stresses in a Cylinder Subjected to an Internal Shock", 2005 Pressure Vessel and Piping Conference, ASME, New York.

[3] Beltman, W. M., Burcsu, E. N., Shepherd, J. E., Zuhal, L., 1999, *The Structural Response of Cylindrical Shells to Internal Shock Loading*, Journal of Pressure Vessel Technology, **121**, ASME, New York, pp. 315-322.

[4] Bayumeister, T., Avallone, E. A., baumeister, t. III, 1978, *Mark's Standard Handbook for Mechanical Engineers,* McGraw Hill, New York.

[5] Keenan, J. H., Keyes, F. G., Hill, P. G., and Moore, J. G., 1969, *Steam Tables*, Wiley, N. Y, p. 104.

[6] ASME B31.3, 1996, Process Piping, ASME, New York.

[7] Streeter,V. L. , and Wylie, E. B., "Fluid Transients in Systems", 1993, Prentice Hall, N. J.

[2] Green, D. J., "Technical Evaluation: 300 Area Steam Line Valve Accident", 1993, Westinghouse, Hanford, Washington.